In vivo phenotypic and molecular characterization of retinal degeneration in mouse models of three ciliopathies

Agnès Brun, Xiangxiang Yu, Cathy Obringer, Daniel Ajoy, Elodie Haser, Corinne Stoetzel, Michel J Roux, Nadia Messaddeq, Hélène Dollfus, Vincent Marion

Experimental Eye Research 186 (2019) 107721

Contents lists available at ScienceDirect

Experimental Eye Research

journal homepage: www.elsevier.com/locate/yexer

In vivo phenotypic and molecular characterization of retinal degeneration in mouse models of three ciliopathies

Agnès Brun[a,1], Xiangxiang Yu[a,1], Cathy Obringer[a], Daniel Ajoy[a], Elodie Haser[a], Corinne Stoetzel[a], Michel J. Roux[b], Nadia Messaddeq[b], Hélène Dollfus[a], Vincent Marion[a,*]

[a] INSERM, Laboratoire de Génétique Médicale, UMR_U1112, Ciliopathies Modeling and Associated Therapies Team (CMAT), Fédération de Médecine Translationnelle de Strasbourg (FMTS), Institut de Génétique Médicale D'Alsace (IGMA), Université de Strasbourg, 11 Rues Humann, Bâtiment 3, 67085, Strasbourg, France
[b] Institut de Génétique et Biologie Moléculaire et Cellulaire (IGBMC), 1 Rue Laurent Fries, 67400, Illkirch-Graffenstaden, France

ARTICLE INFO

Keywords:
Ciliopathies
Unfolded protein response
Retinitis pigmentosa
Bardet-biedl syndrome
Alström syndrome
Leber congenital amaurosis

ABSTRACT

Cilia are highly conserved and ubiquitously expressed organelles. Ciliary defects of genetic origins lead to ciliopathies, in which retinal degeneration (RD) is one cardinal clinical feature. In order to efficiently find and design new therapeutic strategies the underlying mechanism of retinal degeneration of three murine model was compared. The rodent models correspond to three emblematic ciliopathies, namely: Bardet-Biedl Syndrome (BBS), Alström Syndrome (ALMS) and CEP290-mediated Leber Congenital Amaurosis (LCA). Scotopic rodent electroretinography (ERG) was used to test the retinal function of mice, Transmitted Electron microscopy (T.E.M) was performed to assess retinal structural defects and real-time PCR for targeted genes was used to monitor the expression levels of the major apoptotic Caspase-related pathways in retinal extracts to identify pathological pathways driving the RD in order to identify potential therapeutic targets. We found that BBS and CEP290-mediated LCA mouse models exhibit perinatal retinal degeneration associated with rhodopsin mislocalization in the photoreceptor and the induction of an Endoplasmic Reticulum (ER) stress. On the other hand, the tested ALMS mouse model, displayed a slower degeneration phenotype, with no Rhodopsin mislocalization nor ER-stress activity. Our data points out that behind the general phenotype of vision loss associated with these ciliopathies, the mechanisms and kinetics of disease progression are different.

1. Introduction

Ciliopathies, a group of rare genetic diseases, can be either of non-syndromic or syndromic nature in which retinal degeneration (RD) is a cardinal clinical feature (Bujakowska et al., 2017; Estrada-Cuzcano et al., 2012). Ciliopathies contain a spectrum of disorders ranging from isolated RD such as in a sub group of Leber Congenital Amaurosis (LCA) (i.e: Cep290), to complex syndromes with multiple organs dysfunction such as, for example, Bardet-Biedl Syndrome (BBS), Alström Syndrome (ALMS) and the lethal manifestations in the Meckel-Gruber syndrome (Adams et al., 2007; Mockel et al., 2011; Waters and Beales, 2011). These syndromes are caused by mutations in different genes coding for proteins with distinct roles and cellular localizations within the ciliated cells (Cui et al., 2013; Estrada-Cuzcano et al., 2012; Knorz et al., 2010; Reiter and Leroux, 2017). Interestingly, the retinal degeneration presents in many ciliopathies is often of early onset leading to severe visual impairment but can exhibit variable progression phenotypes. For example, RD is characterized by an initial photophobia with nystagmus in Alström syndrome in the first months of life, whereas the first symptoms will be evident only after a few years with nyctalopia and visual field deficiency in BBS (Hamel, 2006; May-Simera et al., 2017). The fact that such differences exist in the RD progression combined with the myriads of mutated genes, lead us to hypothesize that there might be different mechanisms at play at the level of the photoreceptor cell in these different ciliopathies. In view of the heterogeneity, the large number of genes and mutations involved in RD, identifying such mechanistic differences behind these retinal phenotypes is of prime importance in order to properly stratify the patients with future appropriate therapy.

Currently, there is no treatment available for RD; one clinical trial showed the efficacy of gene therapy in LCA (Russell et al., 2017) but it is specific of RPE65 gene mutations. The identification of common

* Corresponding author. INSERM, Ciliopathies Modeling and Associated Therapies Team (CMAT), Laboratory of Medical Genetics (UMRs_U1112), Faculty of Medicine, 11 Rue Humann, Bldg. 3, 9th floor, Room 917, 67085, Strasbourg, France.
E-mail address: vincent.marion@unistra.fr (V. Marion).
[1] These authors contributed equally to the manuscript.

https://doi.org/10.1016/j.exer.2019.107721
Received 25 June 2018; Received in revised form 29 May 2019; Accepted 8 July 2019
Available online 11 July 2019

Table 1
Primers for genotyping PCR.

Gene	Oligo name	Sequence(5′-3′)
Bbs10	4054	ACA AAT ACA ATT GAT CAT CGA TGT G
Bbs10	4057	ACC TCC CCA CTT GAA CGA GGT CT
Bbs10	4058	GTT GCC TGG CTT GGG TGG CA
Cep290	M11336	TGG AAG ACC AGG CTT CAG AG
Cep290	M11340	GGC TCA CTG TGA TCT TGT GC
Cep290	W11338	GTA AGT GCC CGA CAG CTA CC
Cep290	W11339	AGC GCA GTG CAG AGT ATG TG
Rd8	F1	GTGAAGACAGCTACAGTTCTGATC
Rd8	R	GCCCCATTTGCACACTGATGAC
Rd8	F2	GCCCCTGTTTGCATGGAGGAAACTTGGAAGACAGCTACAGTTCTTCTG
Alms	Forward	ACA ACT TTT CAT GGC TCC AGT
Alms	Reverse	TTG GCT CAG AGA CAG TTG AAA

mechanisms could allow the development of therapeutics applicable to RD regardless of the affected gene and the type of mutation. RD in the ciliopathies is linked to the structure of the photoreceptor itself. The photoreceptors outer segment is connected to the inner segment via the connecting cilium (May-Simera et al., 2017; Sjostrand, 1953). This connecting cilium is a protein highway that allows the efficient connection between the biosynthetic active inner segment and the light detecting outer segment for the visual process to start upon photonic impulse. In ciliopathies, ciliary proteins are defective and therefore are no longer able to play their respective roles in the photoreceptor. One of the commonly associated mechanism to photoreceptor apoptosis in the ciliopathies is a defective intraflagellar transport (IFT) of proteins between the two segments (Wright et al., 2010). This defect ultimately causes protein accumulation in the IS, which in turn triggers a pro-apoptotic unfolded protein response (UPR) associated with an ER-stress (Mockel et al., 2012; Starr et al., 2018). Previously, we have proved that UPR activation occurs in a Bbs12 model, leading us to develop a pharmacological approach (GIVin). The treatment slowed RD in our mouse model (Mockel et al., 2012). Other studies targeting non-ciliopathy models have also shown that UPR is an interesting pathway to target in slow RD presenting ER stress. However, RD mechanisms for other emblematic ciliopathies still need to be characterized. We therefore used mice models for three iconic ciliopathies namely BBS, LCA (CEP290) and ALMS to analyze and compare their respective retinal phenotypes while measuring the key components of the UPR pathway.

To date 21 genes (*BBS1-BBS21*) have been identified in BBS (Heon et al., 2016). Half of these proteins are involved in two major BBS protein complexes, the Bbsome complex containing 7 of the BBS proteins (BBS1, 2, 4, 5, 7, 8 and 9) (Nachury et al., 2007) and the BBS-chaperone complex containing three BBS proteins (BBS 6, 10 and 12) (Seo et al., 2010). The pro-apoptotic mechanism of RD associated with Bbs12 has already been characterized in a mouse model (Mockel et al., 2012) and apoptosis was shown to be induced by a deleterious protein accumulation in the IS, leading to the activation of the UPR pathways. We, therefore, determined whether the other BBS proteins could induce the same type of events leading to RD. In the LCA model we studied the centrosomal protein 290 (CEP290), also known as the LCA10 protein, mutations in this gene may lead to various ciliopathies and remarkably a recurrent mutation in intron 26 of CEP290 is a frequent cause of LCA (Garanto et al., 2015). CEP290 protein is known to be involved in photoreceptor development and when mutated leads to early-onset retinal degeneration (Garanto et al., 2015). Finally, in ALMS, only one gene (*ALMS1*) has been identified to date. In human patients, ALMS is characterized by early onset cone-rod dystrophy leading to blindness but the mechanism behind this phenotype remains elusive (Marshall et al., 2007).

2. Material and methods

2.1. Generation of knockout mice and animal husbandry

All experimental procedures were approved by the local ethical committee of Strasbourg University. $Bbs1^{M390R/M390R}$ (henceforth $Bbs1^{-/-}$), $Bbs10^{-/-}$, $Cep290^{-/-}$ and $Alms^{foz/foz}$ mice with their control wild type littermates were generated as described previously (Arsov et al., 2006; Cognard et al., 2015; Davis et al., 2007; Mockel et al., 2012). Stock $Cep290^{tm1.1Jgg}/J$ mice were developed by replacing exons 36, 37 (schematic representation of the mutated allele in Supplementary Fig. 1). Relevant mouse models were bred on a C57BL/6N background and crossbreeding with the C57BL/6J strain to remove the strain-associated interfering Rd8 mutation which interferes with the retinal phenotype (Mattapallil et al., 2012). Mice were kept and bred in humidity- and temperature-controlled rooms on a 12 h light/dark cycle on normal chow and water *ad libitum*. PCR-genotyping were carried out using KAPA Mouse Genotyping Kit (Catalog#KK7302, Kapa Biosystems, Woburn, Massachusetts, USA), primers used for genotyping are listed in Table 1 in supplementary data.

2.2. Electroretinogram

Electroretinograms (ERGs) were performed at the indicated time points with the HMsERG system (Ocuscience®, Kansas City, Missouri, USA). Mice were dark-adapted overnight and then anesthetized by intraperitoneal injection of Domitor® (Medetomidine, 7.6 µg/g body weight) and Ketamine (760 µg/g body weight). The experiments were carried out in dim red light (Catalog #R125IRR, Philips, Suresnes, France). ERGs standard procedure was used according to manufacturer's protocol (Ocuscience®, Kansas City, Missouri, USA). Briefly, the protocol consisted in recording a dark-adapted ERG (Scotopic ERG) after photonic stimuli with intensities ranging from 0.1 to 25 cd s/m^2. ERG results were amplified and captured digitally by ERG View system 4.3 (Ocuscience®, Kansas City, Missouri, USA). The a-wave (corresponding to the first negative deflection) for the scotopic responses was recorded and analyzed.

2.3. Histology and immunofluorescence

Eyeballs were harvested after ERG examination and were fixed 1 h in 4% formalin (Catalog#F5554-4L, Sigma-Aldrich, Saint-Louis, Missouri, USA) at 4 °C, and then incubated sequentially in 10%, 20% and 30% sucrose solutions for 1 h. Eyeballs were then transferred into Optimal Cutting Temperature Compound™ (OCT™, Catalog# 4583, Tissue-Tek® OCT™, Sakura® Finetek, Torrance, California, USA) and frozen in liquid nitrogen. 7 µm cryosections were cut with Cryostat Leica CM1950 (Catalog# 14 0477 8001, Leica Biosystems, Wetzlar, Germany). Eye sections were treated for Haematoxylin-Eosin staining. The thickness of photoreceptor (ONL), inner nuclear layer (INL), outer

Table 2
Antibodies used.

Antibodies	Catalog	Company
Rhodopsin mouse monoclonal	MAB5316	Chemicon
Goat-anti mouse Alexa Fluor® 594	A-11032	Invitrogen

segment (OS) and inner segment (IS) were measured five times at 100 μm regular intervals, the first one was measured at 500 μm distance from the optic nerve. For immunofluorescence, cryosections were post-fixed in 4% formalin for 3 min and then permeabilized with 0.01% TritonX-100 in PBS (Catalog #ET330, Euromedex, France) for 5 min. Sections were incubated 30 min in 1%BSA (Catalog #A7030-100G, Sigma-Aldrich, USA) in PBS at room temperature, then incubated overnight with primary antibodies diluted in blocking buffer at 4 °C. Sections were then incubated for 1 h at room temperature with the secondary antibody. Nuclei were counterstained with Hoechst (#D1306, Invitrogen, Carlsbad, California, USA). Slices were then mounted with Vectashield® Mounting Medium (Catalog #H-1000, Vector Laboratories, Burlingame, California, USA). Images were acquired on a Leica SP8 confocal microscope with either a HC PL APO CS2 63x/1.40 or 40x/1.30 oil immersion lens, driven by the LAS X software (Leica, Weitzlar, Germany). Antibodies used are listed in Table 2 in supplementary data.

2.4. Transmission electron microscopy (T.E.M.)

The samples were fixed by immersion in 2.5% Glutaraldehyde and 2.5% Para-formaldehyde in Cacodylate buffer (0.1M, pH 7.4), post fixed in 1% osmium tetroxide in 0.1M Cacodylate buffer for 1 h at 4 °C and then dehydrated through graded alcohol (50, 70, 90, 100%) and propylene oxide for 30 min each. Samples were embedded in Epon™ 812 (Sigma-Aldrich, Saint-Louis, Missouri, USA). Semi-thin sections were cut at 2 μm with an ultra-microtome (Leica Ultracut UCT, Leica Biosystems, Wetzlar, Germany) and stained with Toluidin blue, and histologically analyzed by light microscopy. Ultrathin sections were cut at 70 nm and contrasted with uranyl acetate and lead citrate and examined at 70 kV with a Morgagni 268D electron microscope. Images were captured digitally by Mega View III camera (Soft Imaging System). The thickness of the photoreceptor ONL, INL and OS + IS were measured five times at 100 μm regular intervals on Toluidin blue stained sections, 3 mice were used for per genotype. Nuclei of ONL were counted, on Toluidin blue stained sections. At least 20 rows were counted in each section and 3 eyes were used for each genotype.

2.5. RNA extraction and real-time PCR

Retinal tissues were harvested as previously described (Mockel et al., 2012). RNA extraction was performed using Trizol® reagent (Catalog #15596-018, Invitrogen®, Life Technologies™, Carlsbad, California, USA) and Tissue Ruptor® (Catalog #9001272, Qiagen, Venlo, Nederland). RNA samples were treated with DNase (TURBO™ DNA-free Kit, Catalog #AM1907, Ambion®, Life Technologies™, Carlsbad, California, USA) prior to reverse transcription using the iScript® cDNA synthesis kit (Catalog#170–889, BioRad, USA). Self-design primers were purchased from Sigma-Aldrich. Quanti-tech Primers were purchased from Qiagen, Courtaboeuf, France (Table 3). Real-Time PCR was performed using the iQ SYBR® Green Supermix (Catalog#170–8886, BioRad, USA) on C1000TM thermo-cycler (CFX96, Real-Time System, Bio-Rad, USA). Real-time PCR was carried out according to the following cycle: initial hold at 95 °C for 30 s and then 39 cycles at 95 °C for 5s and 60 °C for 30s. Quantitative gene expression was calculated by the $2^{\Delta\Delta Ct}$ method relative to the reference gene, *Gapdh*. Primers used for real-time PCR are listed in Table 3 in supplementary data.

Table 3
Primers used for real-time PCR.

Gene	Reference	Company
Mu-Bbs10-Rt-F1	TGCTTAGCAGGGATGGAG	Sigma-Aldrich
Mu-Bbs10-Rt-R1	TTGCAGAGCCTGGGAAATAG	Sigma-Aldrich
Alms1 F	CTGATTTGCCTTTGCTGACA	Sigma-Aldrich
Alms1 R	GCCCTCTGTAAGTGGATGC	Sigma-Aldrich
Caspase3	Mm_Casp3_2_SG QT01164779	Qiagen
Caspase6	Mm_Casp6_2_SG QT00494921	Qiagen
Caspase7	Mm_Casp7_1_SG QT01058085	Qiagen
Caspase9	Mm_Casp9_1_SG QT00133280	Qiagen
Caspase12	Mm_Casp12_2_SG QT00495376	Qiagen
Bip	Mm_Hspa5_1_SG QT00172361	Qiagen
Chop10	Mm_Ddit3_2_SG QT01749748	Qiagen
Perk	Mm_Eif2ak3_1_SG QT00147329	Qiagen
Gapdh	Mm_Gapdh_3_SG QT01658692	Qiagen

2.6. Organotypic culture

The retinas were transferred, with retinal pigmented epithelium side down, to a nitrocellulose culture membrane (catalogue number PICMORG50; Millipore, Molsheim, France) and cultivated as previously described (Mockel et al., 2012). Specific gene silencing with lentiviruses that carried a shRNA sequence for *Alms1* (catalogue numbers sc-108080 (*Ctl*), sc-72345-V (Alms1)); Santa Cruz Biotechnology, Tebu Bio, Yvelines, France) was performed by adding 20 μl of a viral suspension containing 10^5 infectious units to the culture medium overnight. The infected explants were then washed and cultured for 3 days, with half the medium refreshed daily. Explants were not maintained longer in culture to avoid unspecific apoptosis in the different retinal layers.

2.7. Statistical analysis

Student's t-test (two-tailed) was applied to all data (two samples). Statistical tests were performed using GraphPad/Prism version 5. All data in bar charts show mean ± SEM. $p < 0.05$ is considered to have significant differences.

3. Results

3.1. Bbs classical retinal apoptotic phenotype

To assess if mutations in other BBS proteins were inducing RD through the same pro-apoptotic pathophysiological mechanism as the one associated with *Bbs12* (Mockel et al., 2012), two BBS models, *Bbs10*$^{-/-}$ mice model and *Bbs1* $^{M390R/M390R}$ mice model have been characterized and compared. The retinal phenotype for *Bbs1* $^{M390R/M390R}$ has been previously characterized (Davis et al., 2007). In both mice models, histology and RNA analysis were performed on 14-days-old retinas and ERG were performed on 3-month-old mice. 3-month-old *Bbs10*$^{-/-}$ mice showed a significant decrease in light detection capacity measured by ERG compared to control mice (Fig. 1A). Toluidin-blue staining showed that 14-days-old *Bbs10*$^{-/-}$ retina present a significant reduction of the retinal thickness in IS, OS, ONL and INL compared to wild type mice (Fig. 1B, Supplementary Fig. 2A) associated to a decreased of the number of ONL nuclei (Supplementary Fig. 2A). The outer and inner segments of the photoreceptors are completely disorganized but with a correctly formed axonemal microtubules in the connecting cilium as observed by T.E.M (Fig. 1B, Supplementary Fig. 2B) and previously described in *Bbs10*$^{-/-}$ mice (Cognard et al., 2015) and in other BBS mouse models (Davis et al., 2007; Dilan et al., 2018; Hsu et al., 2017; Mockel et al., 2012). In 14-days-old *Bbs10*$^{+/+}$ control retinas, rhodopsin was localized in the OS, while rhodopsin is mislocalized in the IS and the ONL in *Bbs10*$^{-/-}$ retinas (Fig. 1C, Supplementary Fig. 2C). The mRNA levels of key UPR proteins were

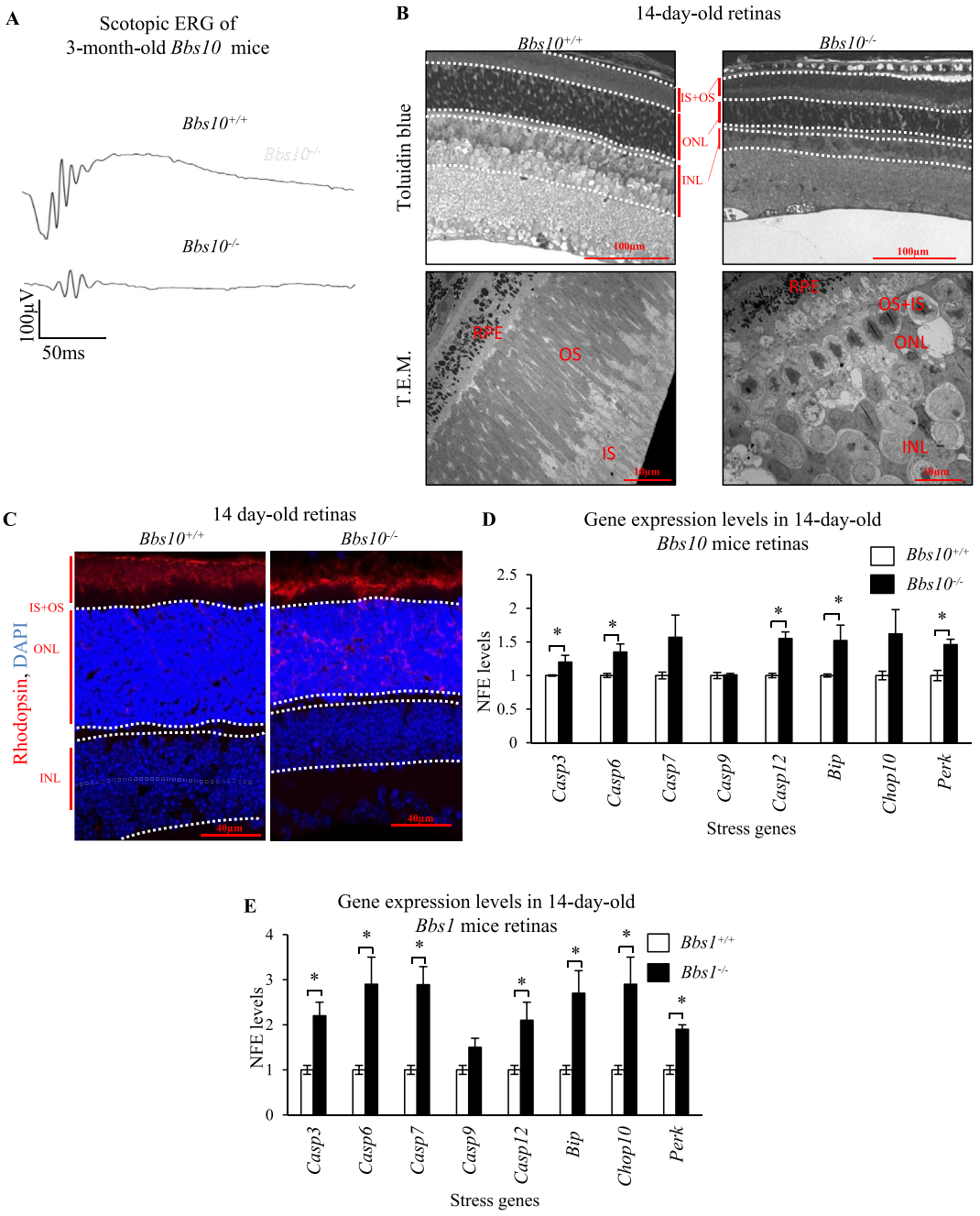

Fig. 1. Retinal phenotype and molecular characterization of *Bbs10* and *Bbs1* mice.
A) Scotopic ERG of 3-month-old *Bbs10* mice (n = 5), *: P ≤ 0.05; B) Toluidin blue staining (Scale bar: 100 µm) and transmission electron microscope (T.E.M) (Scale bar: 10 µm) of 14-day-old *Bbs10* mice retinas (n = 3). RPE: Retinal Pigment Epithelium, OS: Outer Segment: IS: Inner segment, ONL: Outer Nuclear Layer, INL: Inner Nuclear Layer; C) Immunofluorescence of rhodopsin (red) and counterstained nuclei in DAPI on 14-day-old *Bbs10* mice.(n = 3) (Scale bar: 40 µm); D) Stress genes normalized fold expression (NFE) in 14-day-old *Bbs10* mice (n = 3), *: P ≤ 0.05; E) Stress genes NFE in 14-day-old *Bbs1* mice (n = 3), *: P ≤ 0.05. (For interpretation of the references to colour in this figure legend, the reader is referred to the Web version of this article.)

measured in 14-day-old $Bbs10^{-/-}$ mice retinas. Endoplasmic reticulum (ER) stress genes such as *Bip* and *Perk*, are significantly increased in $Bbs10^{-/-}$ mice retinas. *Caspase 12* along with other caspase effectors like *Caspase 3* and *Caspase 6* are also significantly increased (Fig. 1D). Similarly, we characterized the $Bbs1^{-/-}$ mice to confirm the UPR activation as a common mechanism in BBS models. The $Bbs1^{-/-}$ mouse model (Davis et al., 2007) exhibits similar retinal degeneration as the other tested BBS model (*Bbs10* and *12)* (Mockel et al., 2012). The UPR-related set of genes was also upregulated in the 14-day-old $Bbs1^{M390R/M390R}$ retina (Fig. 1E) as in $Bbs10^{-/-}$ retina. These data indicate that the inactivation of the BBS1 protein of the Bbsome triggers the same pro-apoptotic pathway as BBS10.

3.2. LCA-Cep290-mouse model shares the same pro-apoptotic, UPR-mediated mechanism with the Bbs

To verify if this LCA mouse model could share the same pro-apoptotic mechanism as BBS as part of the ciliopathy family, the same experimental approach than BBS was used. At 1-month-old, no ERG signal was detected in $Cep290^{-/-}$ mice. (Fig. 2A). Histological studies at 14 postnatal days on Toluidin-blue stained sections showed a disruption and thinning of retinal layers (IS/OS and ONL) in the $Cep290^{-/-}$ retina

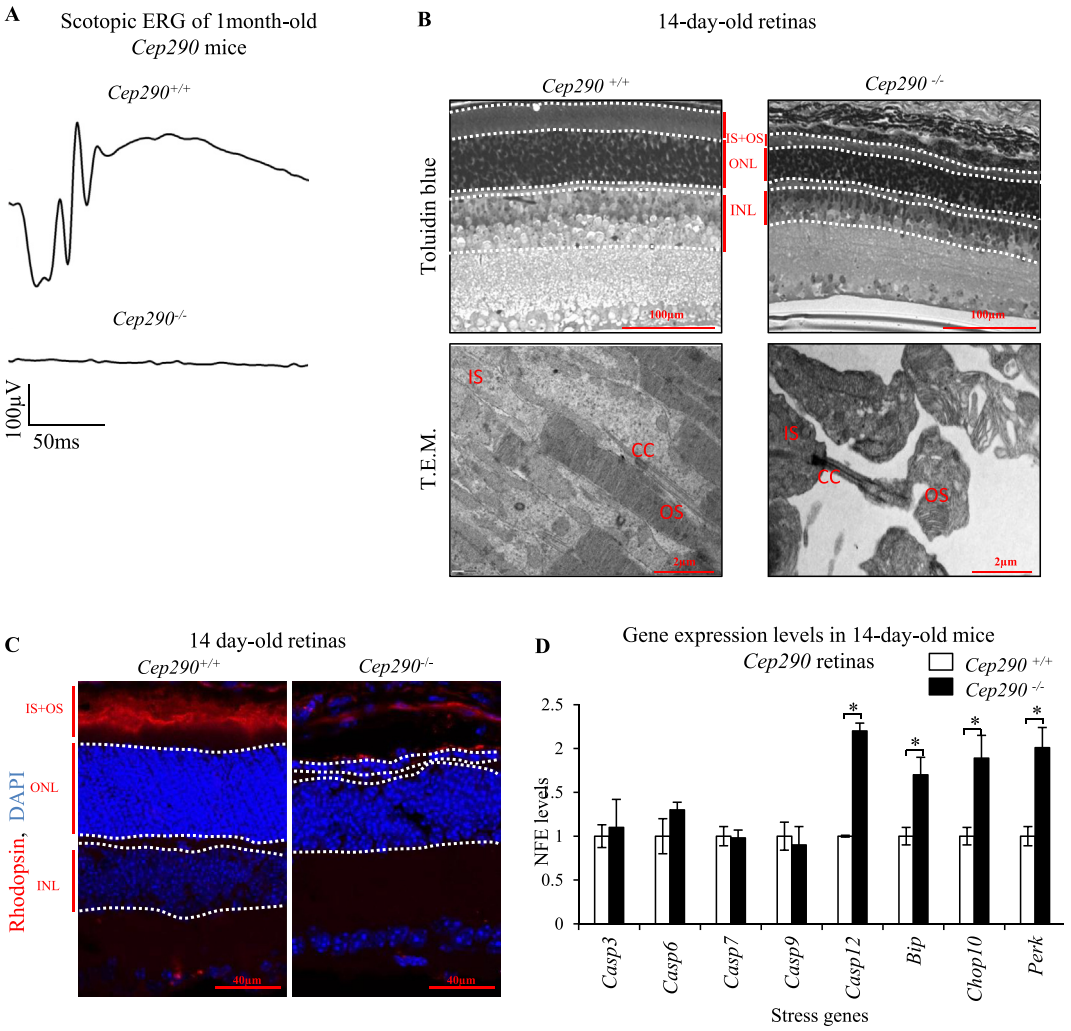

Fig. 2. Retinal phenotype and molecular characterization of *Cep290*$^{-/-}$ mice.
A) Scotopic ERG of 1-month-old *Cep290* mice (n = 3); B) Toluidin blue staining (Scale bar: 100 µm) and T.E.M (Scale bar: 2 µm) of 14-day-old *Cep290* mice retinas. (n = 3) OS: Outer Segment: IS: Inner segment, ONL: Outer Nuclear Layer, INL: Inner Nuclear Layer, CC: Conecting Cilium; C) Immunofluorescence of rhodopsin (red) and counterstained nuclei in DAPI on 14-day-old *Cep290* mice.(n = 3) (Scale bar: 40 µm).). The space between the RPE and the OS is due a detachment of the RPE during preparation.; D) Stress genes NFE in 14-day-old *Cep290* mice retinas *: P ≤ 0.05. (For interpretation of the references to colour in this figure legend, the reader is referred to the Web version of this article.)

(Fig. 2B, Supplementary Fig. 3A). A decrease of nuclei number in the ONL of *Cep290*$^{-/-}$ retina has been observed but it was not statistically significant. T.E.M. analysis revealed the presence of a normal axomal microtubules of the connecting cilium without intact photoreceptors outer segment (Fig. 2B, Supplementary Fig. 3B), which correlates with no ERG signal in *Cep290*$^{-/-}$ mice. On 14-day-old *Cep290*$^{+/+}$ control retinas, immunostaining for rhodopsin showed that rhodopsin localizes in the OS. In contrast, on 14-day-old *Cep290*$^{-/-}$ retinas, rhodopsin was observed in the limits between IS and ONL and in the ONL (Fig. 2C, Supplementary Fig. 3C). The exact location is complicated pinpoint as the IS and OS are severely decreased. At this same age, an upregulation of key genes of the UPR pathway namely *Bip*, *Chop10*, *Perk* and *Caspase12* (Fig. 2D) is also observed in the retinas of *Cep290*$^{-/-}$ mice.

3.3. *Alms1*$^{foz/foz}$ retinal degeneration phenotype

Next, we focused on the retinal phenotype associated with the ALMS syndrome. We investigated the retinal phenotype in the spontaneous mutant mouse line, the Fattie Aussie mouse (*Alms1*$^{foz/foz}$) (Arsov et al., 2006). Interestingly, the ERG measurements in 1-month-old *Alms1*$^{foz/foz}$ mice did not present any significant attenuation of scotopic ERG responses compared to wild type mice at the same age (Fig. 3A). The ERGs were consistent with the retinal morphology; no difference in retinal thickness was observed in 1-month-old *Alms1*$^{foz/foz}$ versus control *Alms1*$^{+/+}$ on retinas H&E staining (Fig. 3B and C). On the other hand, flat electroretinograms were obtained in 1-year-old *Alms1*$^{foz/foz}$ (Fig. 3D), suggesting a slow degenerative process of the retina. Concomitantly, significant thinning of the IS/OS and ONL was measured in 1-year-old *Alms1*$^{foz/foz}$ (Fig. 3E and F). In order to identify any temporal tipping point in the ALMS-related retinal phenotype, we monitored the a-wave amplitude of scotopic ERGs, through time over a 9-month period (Fig. 3G). Interestingly, the a-wave amplitude of the *Alms1*$^{foz/foz}$ rapidly decreased through time. By plotting the a-wave amplitude evolution for the two genotypes, we identified an intersecting point at 7 weeks. We thus started focusing on the *Alms1*$^{foz/foz}$ retinas at 7 weeks postnatal. T.E.M analysis of the *Alms1*$^{foz/foz}$ photoreceptors revealed swelling of the IS together with the presence of vacuoles in the cytoplasm as indicated by asterisks (Fig. 4A) and an intact axonemal structure of the connecting cilium in photoreceptors (Supplementary Fig. 4A). Rhodopsin transport was maintained in *Alms1*$^{foz/foz}$ retina, as rhodopsin was primarily detected in the OS of the photoreceptor (Fig. 4B, Supplementary Fig. 4B). Real-time PCR on the 7-week-old

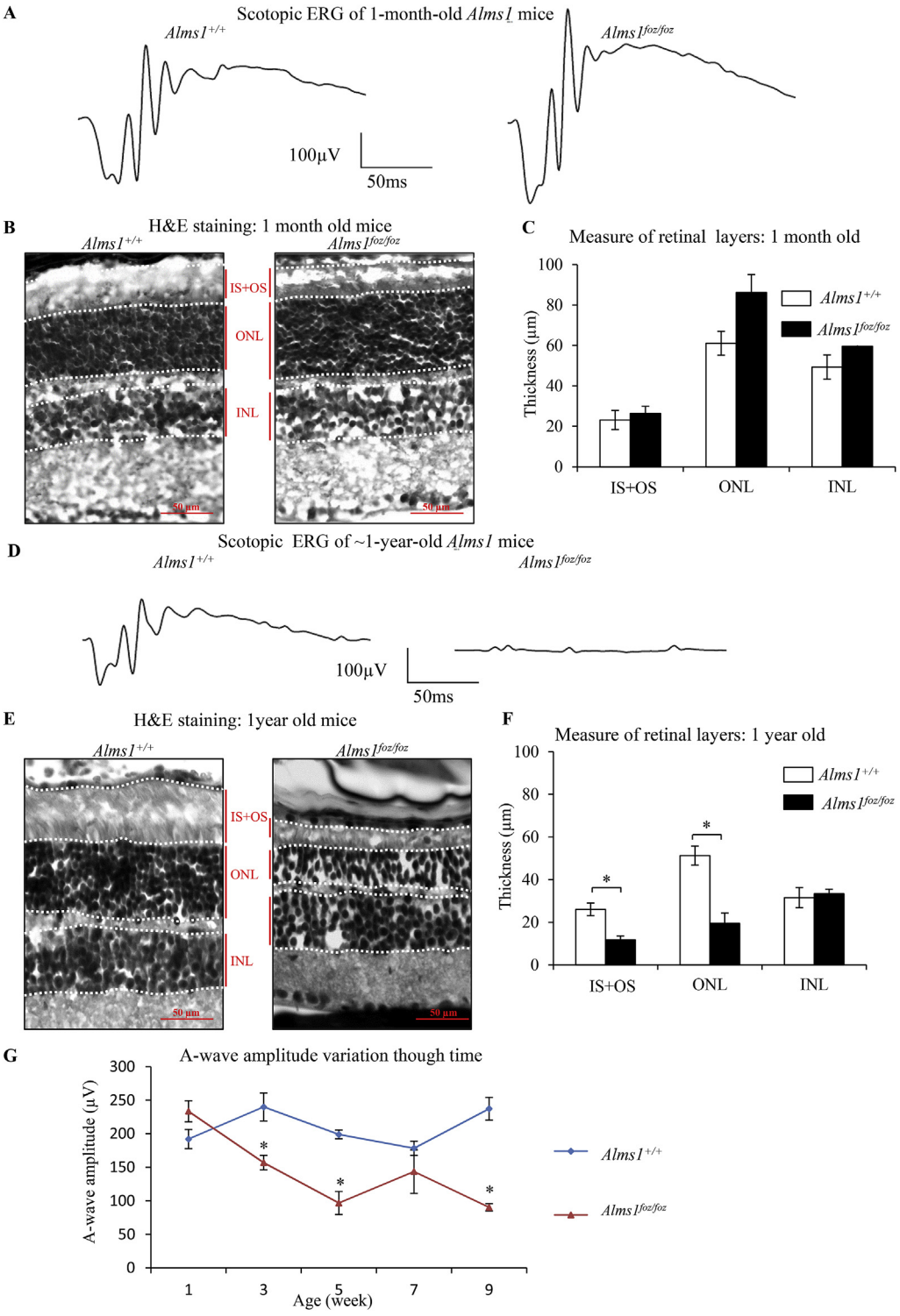

Fig. 3. Retinal phenotype and molecular characterization of *Alms1*$^{foz/foz}$ mice.
A) Scotopic ERGs recording showed retinal function of *Alms1*$^{+/+}$ and *Alms1*$^{foz/foz}$ mice at 1 month-old. B&C). H&E staining (Scale bar: 50 µm) and retinal thickness measurement of 1 month-old *Alms1*$^{+/+}$ and *Alms1*$^{foz/foz}$ mice retinas (n = 3) OS: Outer Segment: IS: Inner segment, ONL: Outer Nuclear Layer, INL: Inner Nuclear Layer; D) Scotopic ERGs recording showed retinal function of *Alms1*$^{+/+}$ and *Alms1*$^{foz/foz}$ mice at 1-year-old. E& F) H&E staining (Scale bar: 50 µm) and retinal thickness measurement of 1-year-old *Alms1*$^{+/+}$ and *Alms1*$^{foz/foz}$ mice retinas (n = 3), *: P ≤ 0.05. G) Evolution of the ERG a-wave amplitude as a function of age for *Alms1*$^{+/+}$ and *Alms1*$^{foz/foz}$ mice.

retinas for the key UPR genes did not show any significant difference in expression level in *Alms1*$^{foz/foz}$ (Fig. 4C) suggesting that the associated phenotype was not linked to the UPR pathways.

Next, we used the organotypic culture approach and culture 14-day-old WT retinas to knock-down *Alms*1 using a lentiviral approach as previously performed (Mockel et al., 2012). 3 days post-infection, real-time PCR analysis showed a 40% decrease in *Alms1* expression level (Fig. 4D) with no difference in expression level of the key UPR-related genes (Fig. 4E) as expected without total absence of *Alms1*. The ALMS-mediated retinal degeneration in the *Alms1*$^{foz/foz}$ mice is not primarily UPR-related.

4. Discussion

RD associated with ciliopathies leads to major visual impairment and understanding the underlying pathogenesis is a prerequisite to define therapeutic options. Describing the pro-apoptotic mechanism underlying ciliopathy-related RD will help to design the therapeutic agents that could hamper the degeneration. With this aim, we studied different murine models for three emblematic ciliopathies, and

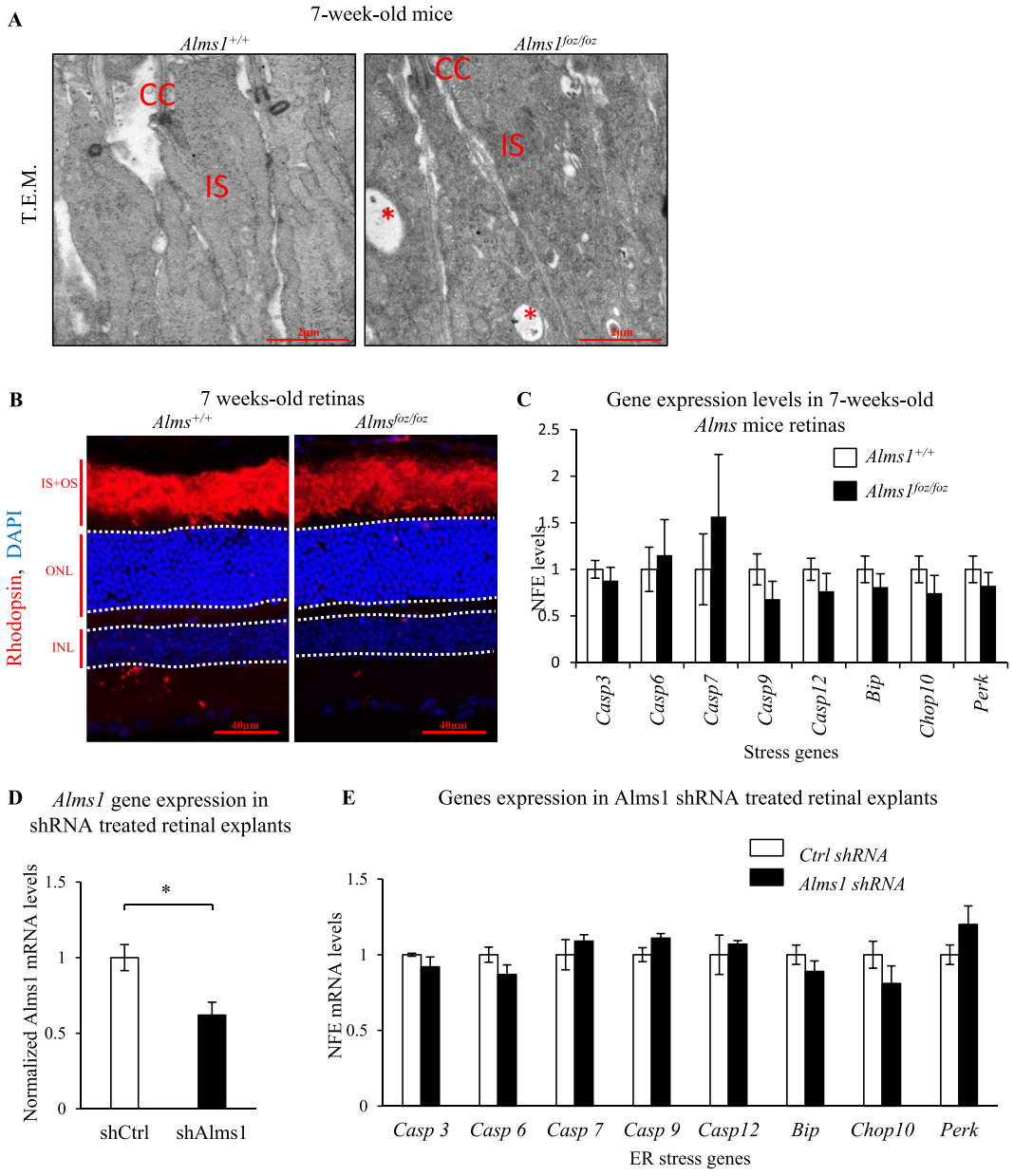

Fig. 4. Ultrastructure of retinas and pathogenic genes expression in 7-week-old *Alms1*$^{foz/foz}$ mice retinas.
A) T.E.M. of 7-week-old *Alms1* mice retina (n = 3) (Scale bar: 2 µm), asterisks indicate the presence of vacuoles in the IS cytoplasm CC: Connecting Cilium; B) Immunofluorescence of localization of rhodopsin (red) and counterstained nuclei in DAPI at 7-week-old on Alms1 mice retina. (n = 3) (Scale bar: 40 µm). OS: Outer Segment: IS: Inner segment, ONL: Outer Nuclear Layer, INL: Inner Nuclear Layer; C) ER stress genes expressions in 7 week-old *Alms1* mice retina (n = 3). D) *Alms1* gene expression in shRNA treated retinal explants (n = 3), *: P ≤ 0.05. E) Stress genes NFE in *Alms1* shRNA treated retinal explants (n = 3), *: P ≤ 0.05. (For interpretation of the references to colour in this figure legend, the reader is referred to the Web version of this article.)

interestingly we could differentiate between UPR-related RD, including the Cep290-LCA and three tested BBS mouse models, and non-UPR-related RDs, namely the ALMS mouse model. Interestingly, the progression rate and the severity of the retinal phenotype in these different mouse models of ciliopathies might be related the UPR pathway as indeed the two UPR-related ciliopathies (BBS and LCA) showed a faster retinal degeneration compared to the ALMS UPR-independent ciliopathies.

Our results showed that, associated to Rhodopsin trafficking defect, key components of the ER stress response were upregulated on the transcriptional level that depicts a common mechanism linked to retinal degeneration in BBS syndromes and LCA, the *Bbs1* $^{M390R/M390R}$ mice, *Bbs10*$^{-/-}$ mice and *Cep290*$^{-/-}$ mice models used herein; although further studies are required to verify this impact on the post-transcriptional level. These mechanisms were also present in *Bbs12*$^{-/-}$ mice model, in the *Rd16* mouse model; a LCA mice model (Mockel et al., 2012; Starr et al., 2018). In *Bbs4*$^{-/-}$ mice models ER stress has not been reported to date even though a Rhodopsin trafficking is already known (Abd-El-Barr et al., 2007). Moreover, the *Cep290*$^{-/-}$ mouse model of LCA was also shown to present ER stress similar to the BBS models showing a possible common mechanism for the RD. *Bbs10*$^{-/-}$ and *Cep290*$^{-/-}$ show a decrease of the different retinal layers at 14 days depicting nuclei loss; with a more significant decrease in *Bbs10*$^{-/-}$ compared to *Cep290*$^{-/-}$. This more aggressive BBS phenotype correlates with a significant drop in nuclear count compared to a smaller drop in *Cep290*. On the other hand, the related phenotype in ALMS model seems UPR unrelated as no upregulation of key players for UPR was observed. Other recent studies suggested that retinopathy in

the Alström syndrome might be linked to a defect in the phototransduction cascade (Hostelley et al., 2016). Indeed the related genes were upregulated in embryos of *Alms1* mutant zebrafish, while this was not significant in BBS1 mutant zebrafish (Hostelley et al., 2016). We also showed that while all retina layers are decreased in the 14-day-old $Bbs10^{-/-}$ and $Cep290^{-/-}$ mice, the INL is not decreased in the $Alms1^{foz/foz}$ mice. It could be caused by a delay in the retinal degeneration and we may hypothesize that the INL will be decrease at a later stage on the disease.

The results above further indicate that retinopathy in ciliopathies may be caused by different mechanisms albeit they exhibit similarity and overlap of retinal phenotypes, and clinical intervention in the future should be given based on precise mechanism dissection. It is known that the retinal phenotypes of ciliopathies show large heterogeneity within the same diseases (Scheidecker et al., 2015). For example, it is well known that the BBS syndrome is a genetically heterogeneous disease. Clinical observation showed that BBS1 patients display a milder and a relatively slower rate of retinal degeneration than that caused by other BBS gene mutations (Daniels et al., 2012); an hypothesis that is supported by the fact that $Bbs1^{M390R/M390R}$ knock-in mice exhibit a relatively slow rate of retinal degeneration compared to other BBS mice models (Cognard et al., 2015; Davis et al., 2007; Mockel et al., 2012). For the LCA, the retinal phenotypes of mouse models of LCA caused by different mutations in different genes (not all associated with ciliopathies) showed large variability in the onset and the courses of diseases, the manifestations of retinal fundus, the pattern of dystrophy (cone-rod dystrophy or rod-cone dystrophy).

The major findings here suggest that it is likely to develop a common therapeutic strategy for retinal dystrophy when ER stress is present, regardless of the causing mutation. In our previous research we demonstrated that treatment targeted at ER stress using *GIVin* could rescue retinal function and retinal morphology in $Bbs12^{-/-}$ mice (Mockel et al., 2012). Other studies have also aimed at developing treatment options for common processes instead of targeting directly the defective gene, this is the case of tauroursodeoxycholic acid (TUDCA) or antioxidants (Drack et al., 2012; Komeima et al., 2007). The vast heterogeneity of the mutations causing RP coupled with the fact that there is not always a proper genetic diagnostic for all the patients make targeted gene therapy a difficult approach. Therefore, the study and development of drugs that can be used in several RP causing situations might be the best option for maintaining PR function for as long as possible, creating a wider therapeutic window for the use of specific treatments for the causing mutations or allowing a better genetic diagnosis in patients with uncommon mutations where the causing defect has not been determined.

Conflicts of interest

All authors declare no conflict of interest.

Acknowledgements

The authors thank all the patient associations for their constant support. This research was supported by Retina France, France; Formicoeur, France; UNADEV, France; Inserm, France; and the University of Strasbourg, France.

Appendix A. Supplementary data

Supplementary data to this article can be found online at https://doi.org/10.1016/j.exer.2019.107721.

References

Abd-El-Barr, M.M., Sykoudis, K., Andrabi, S., Eichers, E.R., Pennesi, M.E., Tan, P.L., et al., 2007. Impaired photoreceptor protein transport and synaptic transmission in a mouse model of Bardet-Biedl syndrome. Vis. Res. 47 (27), 3394–3407. https://doi.org/10.1016/j.visres.2007.09.016.

Adams, N.A., Awadein, A., Toma, H.S., 2007. The retinal ciliopathies. Ophthalmic Genet. 28 (3), 113–125. https://doi.org/10.1080/13816810701537424.

Arsov, T., Silva, D.G., O'Bryan, M.K., Sainsbury, A., Lee, N.J., Kennedy, C., et al., 2006. Fat aussie–a new Alstrom syndrome mouse showing a critical role for ALMS1 in obesity, diabetes, and spermatogenesis. Mol. Endocrinol. 20 (7), 1610–1622. https://doi.org/10.1210/me.2005-0494.

Bujakowska, K.M., Liu, Q., Pierce, E.A., 2017. Photoreceptor cilia and retinal ciliopathies. Cold Spring Harb. Perspect. Biol. https://doi.org/10.1101/cshperspect.a028274.

Cognard, N., Scerbo, M.J., Obringer, C., Yu, X., Costa, F., Haser, E., et al., 2015. Comparing the Bbs10 complete knockout phenotype with a specific renal epithelial knockout one highlights the link between renal defects and systemic inactivation in mice. Cilia 4, 10. https://doi.org/10.1186/s13630-015-0019-8.

Cui, C., Chatterjee, B., Lozito, T.P., Zhang, Z., Francis, R.J., Yagi, H., et al., 2013. Wdpcp, a PCP protein required for ciliogenesis, regulates directional cell migration and cell polarity by direct modulation of the actin cytoskeleton. PLoS Biol. 11 (11), e1001720. https://doi.org/10.1371/journal.pbio.1001720. PBIOLOGY-D-13-03195 [pii].

Daniels, A.B., Sandberg, M.A., Chen, J., Weigel-DiFranco, C., Fielding Hejtmancic, J., Berson, E.L., 2012. Genotype-phenotype correlations in Bardet-Biedl syndrome. Arch. Ophthalmol. 130 (7), 901–907. https://doi.org/10.1001/archophthalmol.2012.89 archophthalmol.2012.89.

Davis, R.E., Swiderski, R.E., Rahmouni, K., Nishimura, D.Y., Mullins, R.F., Agassandian, K., et al., 2007. A knockin mouse model of the Bardet-Biedl syndrome 1 M390R mutation has cilia defects, ventriculomegaly, retinopathy, and obesity. Proc. Natl. Acad. Sci. U. S. A. 104 (49), 19422–19427. https://doi.org/10.1073/pnas.0708571104.

Dilan, T.L., Singh, R.K., Saravanan, T., Moye, A., Goldberg, A.F.X., Stoilov, P., Ramamurthy, V., 2018. Bardet-Biedl syndrome-8 (BBS8) protein is crucial for the development of outer segments in photoreceptor neurons. Hum. Mol. Genet. 27 (2), 283–294. https://doi.org/10.1093/hmg/ddx399.

Drack, A.V., Dumitrescu, A.V., Bhattarai, S., Gratie, D., Stone, E.M., Mullins, R., Sheffield, V.C., 2012. TUDCA slows retinal degeneration in two different mouse models of retinitis pigmentosa and prevents obesity in Bardet-Biedl syndrome type 1 mice. Investig. Ophthalmol. Vis. Sci. 53 (1), 100–106. https://doi.org/10.1167/iovs.11-8544.

Estrada-Cuzcano, A., Roepman, R., Cremers, F.P., den Hollander, A.I., Mans, D.A., 2012. Non-syndromic retinal ciliopathies: translating gene discovery into therapy. Hum. Mol. Genet. 21 (R1), R111–R124 dds298 [pii] 10.1093/hmg/dds298.

Garanto, A., Duijkers, L., Collin, R.W., 2015. Species-dependent splice recognition of a cryptic exon resulting from a recurrent intronic CEP290 mutation that causes congenital blindness. Int. J. Mol. Sci. 16 (3), 5285–5298. https://doi.org/10.3390/ijms16035285.

Hamel, C., 2006. Retinitis pigmentosa. Orphanet J. Rare Dis. 1, 40 1750-1172-1-40 [pii] 10.1186/1750-1172-1-40.

Heon, E., Kim, G., Qin, S., Garrison, J.E., Tavares, E., Vincent, A., et al., 2016. Mutations in C8ORF37 cause Bardet biedl syndrome (BBS21). Hum. Mol. Genet. 25 (11), 2283–2294. https://doi.org/10.1093/hmg/ddw096.

Hostelley, T.L., Lodh, S., Zaghloul, N.A., 2016. Whole organism transcriptome analysis of zebrafish models of Bardet-Biedl Syndrome and Alstrom Syndrome provides mechanistic insight into shared and divergent phenotypes. BMC Genomics 17, 318. https://doi.org/10.1186/s12864-016-2679-1.

Hsu, Y., Garrison, J.E., Kim, G., Schmitz, A.R., Searby, C.C., Zhang, Q., et al., 2017. BBSome function is required for both the morphogenesis and maintenance of the photoreceptor outer segment. PLoS Genet. 13 (10), e1007057. https://doi.org/10.1371/journal.pgen.1007057.

Knorz, V.J., Spalluto, C., Lessard, M., Purvis, T.L., Adigun, F.F., Collin, G.B., et al., 2010. Centriolar association of ALMS1 and likely centrosomal functions of the ALMS motif-containing proteins C10orf90 and KIAA1731. Mol. Biol. Cell 21 (21), 3617–3629. https://doi.org/10.1091/mbc.E10-03-0246 E10-03-0246. ([pii]).

Komeima, K., Rogers, B.S., Campochiaro, P.A., 2007. Antioxidants slow photoreceptor cell death in mouse models of retinitis pigmentosa. J. Cell. Physiol. 213 (3), 809–815. https://doi.org/10.1002/jcp.21152.

Marshall, J.D., Beck, S., Maffei, P., Naggert, J.K., 2007. Alstrom syndrome. Eur. J. Hum. Genet. 15 (12), 1193–1202. https://doi.org/10.1038/sj.ejhg.5201933.

Mattapallil, M.J., Wawrousek, E.F., Chan, C.C., Zhao, H., Roychoudhury, J., Ferguson, T.A., Caspi, R.R., 2012. The Rd8 mutation of the Crb1 gene is present in vendor lines of C57BL/6N mice and embryonic stem cells, and confounds ocular induced mutant phenotypes. Investig. Ophthalmol. Vis. Sci. 53 (6), 2921–2927. https://doi.org/10.1167/iovs.12-9662.

May-Simera, H., Nagel-Wolfrum, K., Wolfrum, U., 2017. Cilia - the sensory antennae in the eye. Prog. Retin. Eye Res. https://doi.org/10.1016/j.preteyeres.2017.05.001.

Mockel, A., Obringer, C., Hakvoort, T.B., Seeliger, M., Lamers, W.H., Stoetzel, C., et al., 2012. Pharmacological modulation of the retinal unfolded protein response in Bardet-Biedl syndrome reduces apoptosis and preserves light detection ability. J. Biol. Chem. 287 (44), 37483–37494. https://doi.org/10.1074/jbc.M112.386821.

Mockel, A., Perdomo, Y., Stutzmann, F., Letsch, J., Marion, V., Dollfus, H., 2011. Retinal dystrophy in Bardet-Biedl syndrome and related syndromic ciliopathies. Prog. Retin. Eye Res. 30 (4), 258–274. https://doi.org/10.1016/j.preteyeres.2011.03.001.

Nachury, M.V., Loktev, A.V., Zhang, Q., Westlake, C.J., Peranen, J., Merdes, A., et al., 2007. A core complex of BBS proteins cooperates with the GTPase Rab8 to promote ciliary membrane biogenesis. Cell 129 (6), 1201–1213 S0092-8674(07)00534-X [pii] 10.1016/j.cell.2007.03.053.

Reiter, J.F., Leroux, M.R., 2017. Genes and molecular pathways underpinning ciliopathies. Nat. Rev. Mol. Cell Biol. https://doi.org/10.1038/nrm.2017.60.

Russell, S., Bennett, J., Wellman, J.A., Chung, D.C., Yu, Z.F., Tillman, A., et al., 2017.

Efficacy and safety of voretigene neparvovec (AAV2-hRPE65v2) in patients with RPE65-mediated inherited retinal dystrophy: a randomised, controlled, open-label, phase 3 trial. Lancet 390 (10097), 849–860. https://doi.org/10.1016/S0140-6736(17)31868-8.

Scheidecker, S., Hull, S., Perdomo, Y., Studer, F., Pelletier, V., Muller, J., et al., 2015. Predominantly cone-system dysfunction as rare form of retinal degeneration in patients with molecularly confirmed bardet-biedl syndrome. Am. J. Ophthalmol. 160 (2), 364–372. https://doi.org/10.1016/j.ajo.2015.05.007. e361.

Seo, S., Baye, L.M., Schulz, N.P., Beck, J.S., Zhang, Q., Slusarski, D.C., Sheffield, V.C., 2010. BBS6, BBS10, and BBS12 form a complex with CCT/TRiC family chaperonins and mediate BBSome assembly. Proc. Natl. Acad. Sci. U. S. A. 107 (4), 1488–1493. https://doi.org/10.1073/pnas.0910268107 0910268107. ([pii]).

Sjostrand, F.S., 1953. The ultrastructure of the outer segments of rods and cones of the eye as revealed by the electron microscope. J. Cell. Physiol. 42 (1), 15–44. Retrieved fromhttp://www.ncbi.nlm.nih.gov/pubmed/13084705.

Starr, C.R., Pitale, P.M., Gorbatyuk, M., 2018. Translational attenuation and retinal degeneration in mice with an active integrated stress response. Cell Death Dis. 9 (5), 484. https://doi.org/10.1038/s41419-018-0513-1.

Waters, A.M., Beales, P.L., 2011. Ciliopathies: an expanding disease spectrum. Pediatr. Nephrol. 26 (7), 1039–1056. https://doi.org/10.1007/s00467-010-1731-7.

Wright, A.F., Chakarova, C.F., Abd El-Aziz, M.M., Bhattacharya, S.S., 2010. Photoreceptor degeneration: genetic and mechanistic dissection of a complex trait. Nat. Rev. Genet. 11 (4), 273–284. https://doi.org/10.1038/nrg2717.